

RESEARCH ACTIVITIES II

Department of Molecular Structure

II-A Development of Near-Field Dynamic Spectroscopy and Application to Nanometric Systems

There is much demand for the study of local optical properties of molecular assemblies and materials, to understand mesoscopic phenomena and/or to construct optoelectronic devices in nanometric scale. Scanning near-field optical microscopy (SNOM), which enables spatial resolution beyond the diffraction limit of light, shows remarkable progress in technology in these days. Combination of this advanced optical technology with ultrafast spectroscopic methods may offer a direct probe of molecular dynamical processes in mesoscopic systems. It may bring essential and basic knowledge for analyzing origins of characteristic features and functionalities of mesoscopic systems. We are constructing apparatus for near-field dynamic spectroscopy with femtosecond temporal resolution and nanometer spatial resolution. Using the apparatus developed, we have observed characteristic spatiotemporal behavior of various organic molecular systems and metal nanoparticles, for the purpose of understanding spatial coherence and dissipation of excitations and their dynamics. Outlines of the construction and experimental results obtained are summarized here.

II-A-1 Scanning Near-Field Optical Microscopy with Supercontinuum Light Pulses Generated in Microstructure Fiber

NAGAHARA, Tetsuhiko; IMURA, Kohei;
OKAMOTO, Hiromi

[*Rev. Sci. Instrum.* **75**, 4528–4533 (2004)]

We have utilized supercontinuum (SC) pulses as a light source for SNOM experiments with high spatial-resolution (~ 100 nm) determined by the aperture size of the near-field probe. The SC ranging from 560 nm to > 1 μm is generated by focusing mode-locked Ti:sapphire laser pulses into a microstructure fiber. The continuum can be used as a wavelength-tunable light source for fluorescence excitation as well as for probing absorption of excited states.

To examine performance and versatility of the apparatus, fluorescence image of pseudoisocyanine J-aggregate was measured. The sample was illuminated through the apertured tip by spectrally-sliced SC at 560 nm. Fluorescence from the sample (at 590 nm) was detected by an avalanche photodiode. Fluorescence (Figure 1A) and topographic (not shown) images correlate very well. The images show that the J-aggregates have fibrous structures, in agreement with earlier works. The fluorescence image is in some parts noisy and smeared. The noisy signal is coming from fluctuation of the SC, and quality of the fluorescence image would be much improved by stabilizing the incident Ti:sapphire laser.

Next we describe two-color pump-probe measurements using SC. Time resolution in the near-field with near-IR probe pulse was in 1–2 ps range, while that with 570 nm pulse was 5 ps without pre-compensation of group delay dispersion. As an example, we have measured a thin film of porphyrin J-aggregates. Signals from spectrally sliced SC at 810 nm after excitations at 780 nm are shown in Figure 1C, together with the topography (Figure 1B) of the sample. The lifetimes at

positions specified in the topograph (112 ± 6 ps and 79 ± 6 ps) show clear site dependence. The site-specificities in excited-state dynamics have been revealed in the present *two-color* experiment much more clearly compared to our previous *one-color* result,¹⁾ since the baselines are directly determined from intensities at negative delay times.

Reference

- 1) T. Nagahara, K. Imura and H. Okamoto, *Chem. Phys. Lett.* **381**, 368–375 (2003).

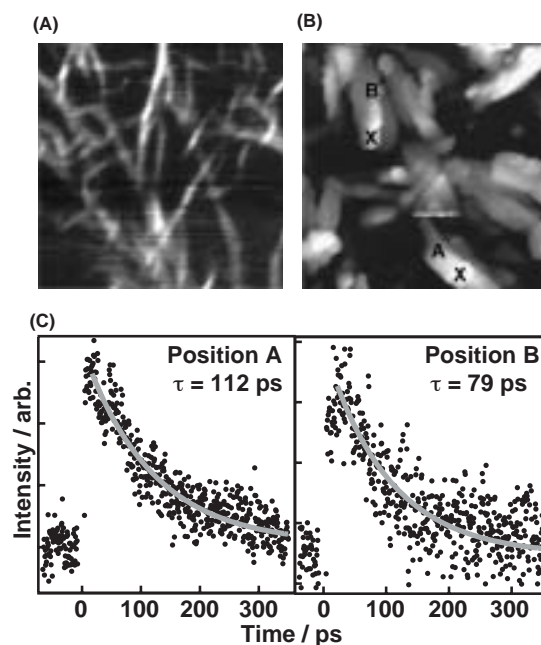


Figure 1. (A) Fluorescence image of PIC J-aggregate detected at 590 nm. Scan range: $10 \mu\text{m} \times 10 \mu\text{m}$. (B) Topography of tetrakis(4-methoxyphenyl)porphyrin J-aggregate. Scan range: $5 \mu\text{m} \times 5 \mu\text{m}$. (C) Signals obtained by 780-nm pump / 810-nm probe experiments and their fit to exponential function.

II-A-2 Near-Field Spectroscopy of Water-Soluble and Water-Insoluble Porphyrin J-Aggregates

NAGAHARA, Tetsuhiko; IMURA, Kohei;
OKAMOTO, Hiromi

[*Scanning* **26** (Suppl. I), 10–15 (2004)]

Recently, we examined the mesoscopic structures and spatial inhomogeneities of J-aggregate of water-insoluble tetrakis(4-methoxyphenyl)porphyrin (TMeOPP) in thin film by SNOM. The results obtained were as follows: (a) thin film consists of bundles of long and planer microcrystalline structures; (b) site-specific transmittance spectra might reflect spatial inhomogeneity of the sample, which may be a major origin of the broad J-bands in the far-field spectrum. However, influence of substituent groups on the spatial inhomogeneities and morphologies was not investigated. In the present study, we have studied mesoscopic structures and optical properties of J-aggregates of tetraphenylporphyrins with different substituent groups [unsubstituted (TPP) and 4-sulfonated (TSPP)].

From topographic images, TSPP sample is composed of needle-like planar microcrystals ($\sim 1 \mu\text{m-L}$, $\sim 100 \text{ nm-W}$ and $5\text{--}10 \text{ nm-H}$), while that of TPP (Figure 1B) shows stacks of planer ($300 \sim 600 \text{ nm} \times 300 \sim 600 \text{ nm}$, $\sim 20 \text{ nm-H}$) microcrystalline structures. From polarized transmittance images of TSPP (Figure 1A), it was found that a large transition moment is parallel to the long crystalline axis. Individual microcrystallines in TPP sample have been found to be planer rhomboid structures by SEM observations. Such morphological differences are probably due to microscopic differences in aggregate structures.

In the far-field absorption and fluorescence spectra, the bandwidths of the water-insoluble samples (TPP and TMeOPP) were much broader than that of water-soluble sample (TSPP), suggesting serious contributions of inhomogeneous broadening. The near-field transmittance spectra of the water-insoluble samples show strong site-dependence (Figure 1C), while those of the water-soluble ones do not. The origin of the broad absorption band observed in water-insoluble samples can be ascribed to spatial inhomogeneities.

Reference

- 1) T. Nagahara, K. Imura and H. Okamoto, *Chem. Phys. Lett.* **381**, 368–375 (2003).

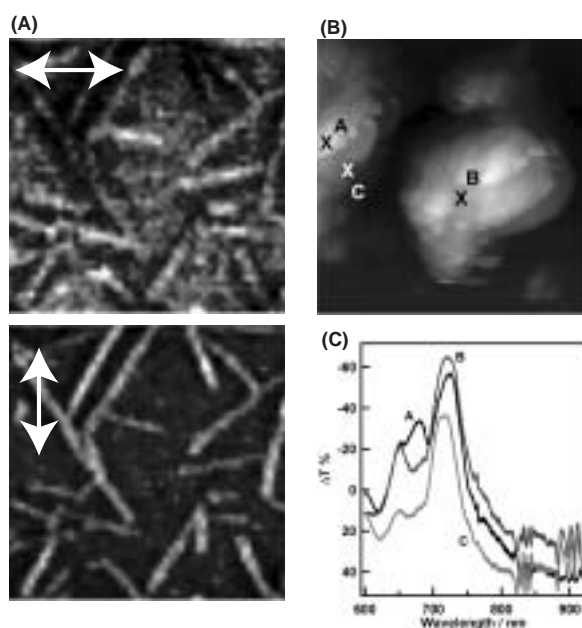


Figure 1. (A) Polarized transmittance image of TSPP J-aggregate. Arrows indicate polarization directions. Scan range: $2 \mu\text{m} \times 2 \mu\text{m}$. (B) Surface topography of TPP J-aggregate. Scan range: $5 \mu\text{m} \times 5 \mu\text{m}$. (C) Transmittance difference spectra at positions indicated in (B).

II-A-3 Near-Field Optical Observation of Gold Nanoparticles

IMURA, Kohei; NAGAHARA, Tetsuhiko;
OKAMOTO, Hiromi

[*Chem. Phys. Lett.* **400**, 500–505 (2004)]

Optical properties of noble metal particles have been widely investigated because of fundamental importance in science and in industry. Not only the local field enhancement but also the SP mode behaviors in near-field arouse fundamental interests and various applications. Wavelength-dependent characteristics of SP modes on metal nanoparticles are essential for utilizing them as novel optical and electronic materials, and also for constructing molecular systems for nanophotonic applications as well.

We investigated interaction between evanescent wave and a single gold nanoparticle in near-field by utilizing an aperture-probe SNOM. A characteristic spectral feature, consisting of transmission enhancement and absorptive parts, was found. Observed spectra were successfully simulated by a model calculation based on extended Mie scattering theory of the near- and far-field scatterings as well as by a Green dyadic treatment of electromagnetic field.

II-A-4 Two-Photon Induced Photoluminescence Imaging of Single Gold Particles

IMURA, Kohei; NAGAHARA, Tetsuhiko;
OKAMOTO, Hiromi

[*J. Am. Chem. Soc.* **126**, 12730–12731 (2004)]

Strong field confinement near and/or adjacent particles is important in surface enhanced Raman scattering (SERS). However, knowledge about spatial distribution of electric field near the particle and how plasmon modes play roles in the particle are still not fully understood. We have found that two-photon induced photoluminescence (TPI-PL) of single nanoparticles can be excited in the near-field, and this has been used to reveal spatial distribution of electric field near the particle as well as spatial characteristics of plasmon modes.

Gold nanoparticles were synthesized chemically in solutions by seed-mediated method. Morphology of the sample was verified by topography measurements by the apertured SNOM and/or by a scanning electron microscope. Samples were spin-coated on a cover-slip. A Ti:sapphire laser ($\lambda = 780$ nm, < 100 fs) was used to excite TPI-PL. Laser power dependence measurement of the PL intensity confirmed that PL was due to a two-photon induced process.

Figure 1 (a,b) shows the TPI-PL image of single gold nanorods. Figure 1(a) shows electric field enhancement near the ends of the rod, while Figure 1(b) shows a characteristic spatial oscillation. This oscillatory behavior is well reproduced by an electromagnetic calculation and is ascribed to electromagnetic local density of states which reflect the eigenfunction of certain surface plasmon mode. The origin of the difference between Figures 1(a) and (b) is possibly related to microscopic edge structures of the rod and/or the resonance condition of the plasmon mode at the excitation wavelength.

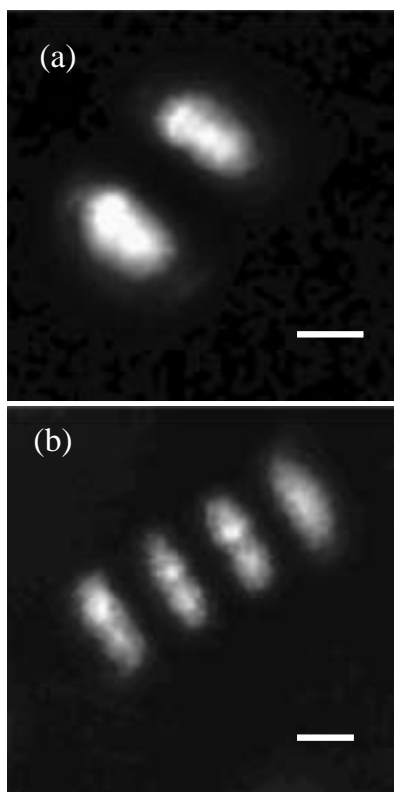


Figure 1. (a,b) Two-photon induced PL images for two typical single gold nanorods. Scale bars are 100 nm.

II-A-5 Ultrafast Near-Field Imaging of Single Gold Nanorods

IMURA, Kohei; NAGAHARA, Tetsuhiko;
OKAMOTO, Hiromi

[*J. Phys. Chem. B* **108**, 16344–16347 (2004)]

We deal with ultrafast dynamics of collective oscillation of electrons, known as surface plasmon (SP), for gold nanorods. The SP modes of nanoparticles give rise to strong interaction with photons. It is of fundamental importance to know how the electron-electron and electron-phonon scattering processes after photoexcitation depend upon size and shape of nanoparticles and how they proceed inside the particle. Dynamical spectroscopy of a single particle with high temporal and spatial resolution must be informative for this purpose. We have performed experiments of ultrafast near-field pump-probe imaging, and investigated the dynamic behavior of the excited particle in a space- and time-resolved manner.

Figure 1 shows transient transmission images of a gold nanorod taken at various pump-probe delay times. As it is clearly seen in the figure, temporal response of central part of the particle is different from those of the both ends. A fast rise and a slow decay are seen for the ends parts, while only a fast rise component is observed for the central part. The time constant for the faster component was found 0.6 ± 0.1 ps and the slower one 2.8–1.5 ps depending on the position inside the particle. The faster and slower components are assigned to electron-electron and electron-phonon scattering, respectively. It is found that the electron-phonon relaxation becomes faster towards the end edge of the nanorod.

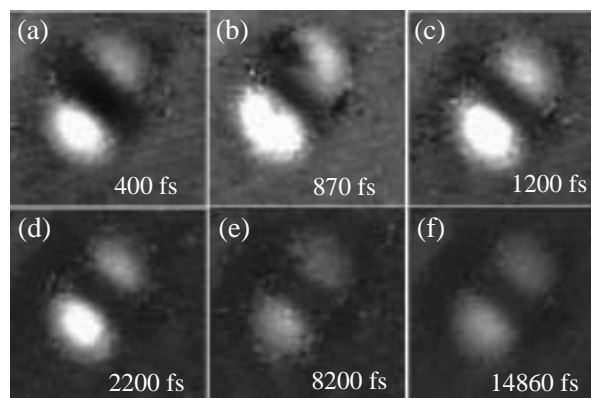


Figure 1. (a–f) Transient transmission images of a gold nanorod taken at various pump-probe delay times (indicated in each image). Scan range: 600 nm \times 600 nm.

II-B Spectroscopic Studies on Atoms and Ions in Liquid Helium

Atoms and ions in liquid helium are known to reside in bubble-like cavities due to the Pauli repulsive force between electrons. Physical properties of these exotic surroundings are determined by the potential energy of the impurity-He_n system, the surface tension energy of the liquid helium, and the pressure-volume work. Spectroscopic studies of such impurity atoms and ions in liquid helium are expected not only to give interesting information on the structure and dynamics of the bubbles but also to contribute to the study on physical properties of superfluid liquid helium.

II-B-1 Laser Spectroscopic Studies of Mg Atoms in Cold Helium Gas

MORIWAKI, Yoshiki¹; MORITA, Norio
(¹Toyama Univ.)

In our previous laser spectroscopic study¹⁾ on Mg atoms in liquid helium, since both the peak shift and width of the emission spectrum of the $3s3p\ ^1P \rightarrow 3s^2\ ^1S$ transition were significantly larger than those expected from a simple bubble model, we inferred that a Mg($3s3p\ ^1P$)He₁₀ exciplex was formed in a bubble, just similar to the case of excited alkaline atoms in liquid helium. Such exciplexes are known to have a characteristic structure in which helium atoms form a ring in the nodal plane of the excited p -electron of an impurity atom, and our theoretical spectrum calculated based on a similar exciplex model showed better agreement with the experimental spectrum in comparison with the one calculated with a simple bubble model. In the case of Mg, however, unlike alkaline atoms, the $3s$ electron lies around the nodal plane of the $3p$ electron, and so there is a possibility that the $3s$ electron prevents helium atoms from forming the ring structure due to the Pauli repulsive force. This means that the formation of the Mg($3s3p\ ^1P$)He₁₀ exciplex is still ambiguous. In the present study, therefore, we have investigated the emission spectrum of Mg atoms in cold helium gas, and have compared it with the calculated spectrum as well as the experimental spectrum obtained for liquid helium. Consequently, as seen in Figure 1, we have found that the spectrum for gaseous helium is in very good agreement with the one calculated based on the model of the Mg($3s3p\ ^1P$)He₁₀ exciplex formation. This result strongly supports our inference that Mg atoms in liquid helium can form Mg($3s3p\ ^1P$)He₁₀ exciplexes in spite of the presence of the $3s$ electron.

Reference

1) Y. Moriwaki and N. Morita, *Eur. Phys. J. D* **5**, 53 (1999).

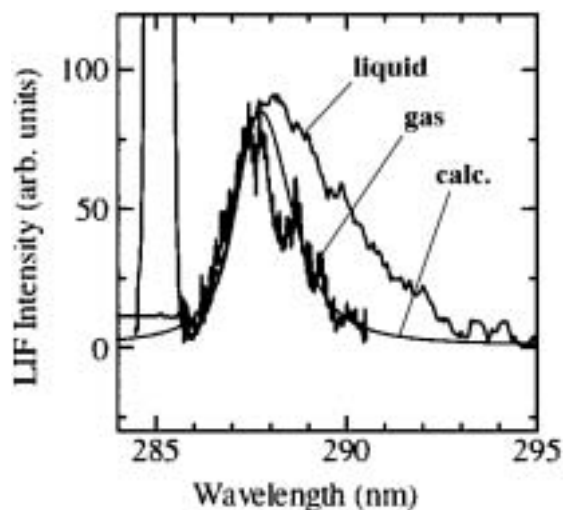


Figure 1. Emission Spectra of Mg atoms in gaseous and liquid helium at 1.4 K. A calculated spectrum is also plotted.

II-B-2 Observation of Remarkable Difference between Mobilities of Impurity Eu atoms in Solid Helium-3 and Helium-4

MORIWAKI, Yoshiki¹; MORITA, Norio
(¹Toyama Univ.)

We have measured emission spectra of Eu atoms in liquid and solid helium at 1.4 K over a wide pressure range across the solidification pressure. Consequently, as seen in Figure 1, we have found that the behavior of the spectral intensity across the solidification pressure remarkably differs between ³He and ⁴He; while for ⁴He the intensity drastically increases above the solidification pressure, no significant change is seen for ³He across the solidification pressure. This difference can be interpreted as a manifestation of the difference in mobility of Eu atoms. Since the helium atom is so light that even its zero-point vibration has a quite large amplitude, the position exchange between neighboring helium atoms frequently occurs even in solid due to the tunnel effect. Therefore, each helium atom in solid helium always moves around, and impurity atoms can also move and diffuse following the motion of helium atoms. No significant change seen for ³He across the solidification pressure means that impurity Eu atoms in solid ³He can diffuse with almost the same mobility as in liquid. On the other hand, the drastic intensity increase seen for ⁴He shows that the mobility of Eu atoms in solid ⁴He is significantly small in comparison with the one in solid

^3He . A possible reason may be the larger mass of ^4He atom, which results in a smaller amplitude of the zero-point vibration. Another possible reason might be that solid ^4He is (partly) a Bose condensate at 1.4 K, while there is no condensate in solid ^3He . In a Bose condensate many helium atoms coherently vibrate, and this might cause the less position exchange between neighboring atoms.

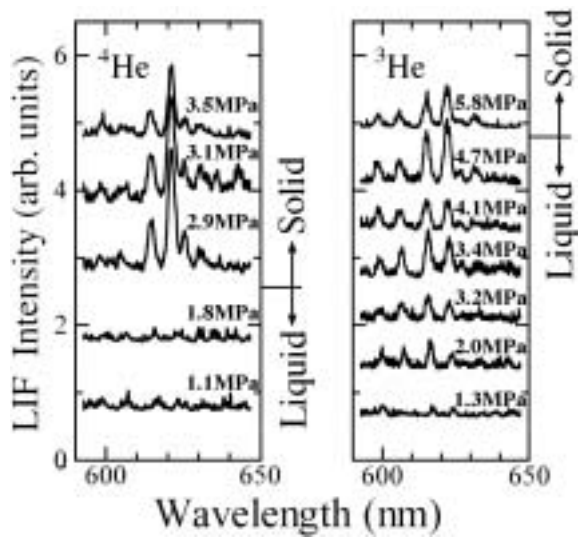


Figure 1. Pressure dependences of emission spectra of Eu atoms in liquid ^3He and ^4He at 1.4 K; liquid ^4He and ^3He at this temperature solidify at about 2.5 and 5.0 MPa, respectively.

II-C Surface Chemical Reactions Studied by NEXAFS Spectroscopy

Recently, we have developed an energy dispersive NEXAFS (Near Edge X-ray Absorption Sine Structure) method, which is a technique to measure a NEXAFS spectrum in a certain range simultaneously. This method shortens the measuring time by 1/100 compared with the conventional energy scanning method and enables us to apply the NEXAFS spectroscopy to surface chemical reactions related to fundamental catalytic reactions. Since the time scale is comparable with STM measurement, combined information of NEXAFS and STM as well as dynamic Monte-Carlo simulations provides deep insight to fundamental chemical reactions which have not been clarified yet. So far, we have applied it to the reactions of water formation reaction/Pt(111) and ammonia formation on Rh(111).

II-C-1 Reaction-Path Switching Induced by Spatial-Distribution Change of Reactants: CO Oxidation on Pt(111)

NAKAI, Ikuyo¹; KONDOH, Hiroshi¹; AMEMIYA, Kenta¹; NAGASAKA, Masanari¹; NAMBU, Akira¹; SHIMADA, Tohru¹; OHTA, Toshiaki²
(¹Univ. Tokyo; ²Univ. Tokyo and IMS)

[*J. Chem. Phys.* **121**, 5035 (2004)]

CO oxidation on Pt(111) surfaces is one of the most prototypical catalytic reactions. We studied the mechanism of CO oxidation on O-covered Pt(111) surfaces during CO exposure by means of time-resolved NEXAFS spectroscopy. Recent STM study proposed that the oxidation reaction takes place exclusively at island peripheries after an "induction period" where the reaction does not proceed. However, we found that the whole reaction process is composed of two distinct processes; (1) a reaction of isolated oxygen atoms with adsorbed CO, and (2) a reaction of island-periphery oxygen atoms after the CO saturation. If CO pressure is lowered, these two processes are separated by an induction period, in which CO saturates the O-covered surface. A drastic switching of reaction path in CO oxidation reaction is caused by the CO adsorption induced 2D condensation of the O atoms. These results demonstrate that the effects of long-range interactions and consequent dynamic spatial-distribution changes of the reactants are of fundamental importance for understanding the kinetics in the reaction systems deviated from the conventional Langmuir-Hinshelwood kinetics.

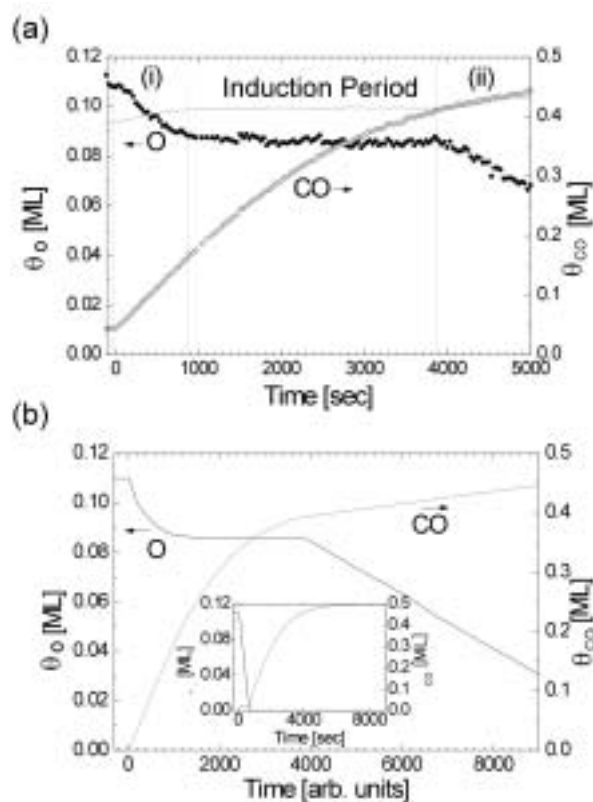


Figure 1. (a) Time evolution of θ_{O} and θ_{CO} under a low pressure of CO (5×10^{-10} Torr). The annealing temperature and the reaction temperature were 260 K and 252 K, respectively. The gray line shows the saturation coverage of CO. The areas (i) and (ii) correspond to the former and latter processes, respectively.

(b) Variation of θ_{O} and θ_{CO} from Monte Carlo simulation under the same condition as for the experiment shown in (a). The solid and dashed lines represent θ_{O} and θ_{CO} , respectively. Inset: Simulated curves without taking account of CO adsorption-induced condensation of O atoms.

II-D Ultrafast Dynamics of Surface Adsorbed Species

Understanding of reaction dynamics at surfaces using ultra-short laser techniques is an important issue to clarify the mechanism of the reactions. Real-time observation of temporal change of surface species induced by UV, visible, and (Near-) infrared pump pulses is carried out using mid-IR pump-probe vibrational spectroscopy and Sum-frequency generation (SFG) spectroscopy which is one of the non-linear spectroscopies using ultra-short laser has high sensitivity for detection of molecular vibrations of adsorbed species on surface in the first layer. The aim of this study is the identification of molecular structures of the intermediates generated by electronic, vibrational, or thermal excitation and understanding of the reaction kinetics including potential energies, activation barriers, and entropies. Typical systems of our recent studies are formate (DCOO) adsorbed on Ni(111) surface, olefins on OH group of zeolite. In addition to the ultrafast observation of surface events, controls of excited states of molecules and chemical reaction are tried using optimized pulse shaping technique. In the study, we succeeded in controlling the two-photon excitation efficiency and selective excitation of excited states of an α -perylene crystal.

II-D-1 Dynamic Processes of Olefins Adsorbed on Hydroxyl Groups of DM20 Zeolite Excited by Picosecond Infrared Pulses

ONDA, Ken¹; TANABE, Kinuka¹; NOGUCHI, Hidenori¹; DOMEN, Kazunari¹; WADA, Akihide²
(¹Tokyo Inst. Tech.; ²IMS and Tokyo Inst. Tech.)

[*J. Phys. Chem. B* **107**, 11391–11396 (2003)]

We have investigated olefins adsorbed on Brønsted acidic hydroxyl groups (OD) of DM20 zeolite by transient infrared absorption spectra after excitation of the OD stretching mode using picosecond infrared lasers. The olefins studied were ethylene, deuterated ethylene, propylene, and isobutene, and only isobutene was adsorbed on OD at its methyl group while the other olefins were adsorbed at their double bonds. For all the olefins except isobutene, simple vibrational relaxation of the $\nu = 1$ state was observed and the lifetimes were 2–4 ps. These lifetimes are an order faster than that of isolated OD. For isobutene, a long lifetime component lasting more than 500 ps was observed in addition to vibrational relaxation of 2 ps. The transient absorption spectra for isobutene-adsorbed zeolite at various time delays and frequencies indicated the existence of a short-lived species and a slow desorption process compared with vibrational relaxation.

II-D-2 Dynamical Response of Formate/Ni(111) System to Picosecond Near Infrared Pulses

NOGUCHI, Hidenori¹; ONDA, Ken¹; OKADA, Takuya¹; KUBOTA, Jun¹; KOBAYASHI, Hisayoshi²; KANO, Satoru S.³; DOMEN, Kazunari¹; WADA, Akihide⁴
(¹Tokyo Inst. Tech.; ²Kurashiki Univ. Sci. Arts; ³Hosei Univ.; ⁴IMS and Tokyo Inst. Tech.)

Time-resolved sum-frequency generation (TR-SFG) spectroscopy was carried out on a deuterated formate (DCOO) adsorbed on Ni(111) surface to investigate the surface reaction dynamics induced by irradiation of picosecond near-infrared laser pulses. The irradiation of pump pulse (800 nm) caused rapid intensity decreases of both CD and OCO stretching modes of bridged formate on Ni(111). Different temporal behaviors of intensity recovery between these two vibrational modes

were observed, *i.e.*, the intensity of CD stretching mode recovered significantly faster than that of OCO symmetric stretching mode. From the results of transient measurements, we concluded that the observed intensity change was mainly due to a transient structural change of formate and we discussed about the mechanisms of the change.

II-D-3 Optical Control of Excited States of α -Perylene Crystal Using Optimized Pulse Shaping Method

MIZOGUCHI, Ryyuichi¹; KANO, Satoru S.²; WADA, Akihide³
(¹Tokyo Inst. Tech.; ²Hosei Univ.; ³IMS and Tokyo Inst. Tech.)

[*Chem. Phys. Lett.* **379**, 319–324 (2003)]

Optical control of excited states of α -perylene crystal was realized by a femtosecond optimized pulse shaping method using Genetic Algorithm (GA). We succeeded in controlling the emission spectral feature of an α -perylene crystal; the intensity of E-emission was increased by a factor of 1.4 without the change of Y-emission intensity. Furthermore, we found a near-infrared pulse shape whose multi-photon excitation efficiency is larger than that of a single femtosecond pulse by a factor of two. On the auto-correlation traces of these shaped pulses, the several satellite peaks appeared beside the main peak. The origin and mechanism of the attained change were discussed.

II-D-4 Optical Control of Two-Photon Excitation Efficiency of α -Perylene Crystal by Pulse Shaping

OKADA, Takuya¹; OTAKE, Ikuya¹; MIZOGUCHI, Ryyuichi¹; ONDA, Ken¹; KANO, Satoru S.²; WADA, Akihide³
(¹Tokyo Inst. Tech.; ²Hosei Univ.; ³IMS and Tokyo Inst. Tech.)

[*J. Chem. Phys.* to be published]

Optimized pulse shaping experiments were carried out on the control of two-photon excitation efficiency of an α -perylene crystal in the temperature region from 30

K to 290 K. It was found that a pulse train with a pulse interval of 90 fs and an alternately reversing phase relation increased the excitation efficiency by a factor of 2 for the whole temperature region. The pulse shape characteristic for effective efficiency increase was deduced by double pulse experiments in which the dependence of the emission intensity on the pulse interval and relative phase between pulses were measured. The mechanism of the efficiency increase is briefly discussed using a sliding-window Fourier transform of the pulse shape.

II-E Structure and Function of Metalloproteins and Its Molecular Design

Metal ion is a common cofactor that is crucial for active centers of proteins involved in many biologically important processes in cells, and a relatively small number of metal-based prosthetic groups are utilized to serve numerous and diverse chemical functions. A typical metal-based prosthetic group, which represents a fascinating example in this respect, is heme. Heme promotes a variety of functions, such as dioxygen storage, activation of small molecules, electron transfer reactions, and sensing gaseous molecule. In the field of protein design and engineering, hemoproteins also make particularly attractive targets. There are many reasons for this, including the exciting possibility of engineering protein-based molecules with useful catalytic, electronic or optoelectronic properties. Based on various kinds of spectroscopies, we have functionally and structurally characterized some hemoproteins including newly identified heme-regulated proteins, and designed hemoproteins showing improved activities and new functions.

II-E-1 Structural and Functional Characterization of "Laboratory Evolved" Cytochrome P450cam Mutants Showing Enhanced Naphthalene Oxygenation Activity

MATSUURA, Koji¹; TOSHA, Takehiko¹;
YOSHIOKA, Shiro¹; TAKAHASHI, Satoshi¹;
ISHIMORI, Koichiro²; MORISHIMA, Isao¹
(¹Kyoto Univ.; ²IMS and Kyoto Univ.)

[*Biophys. Biochem. Res. Commun.* **324**, 1095 (2004)]

To elucidate molecular mechanisms for the enhanced oxygenation activity in the three mutants of cytochrome P450cam screened by 'laboratory evolution' (H. Joo, Z. Lin and Z. F. H. Arnold, *Nature* **399**, 670–673 (1999)), we purified the mutants and characterized their functional and structural properties. The electronic absorption and resonance Raman spectra revealed that the structures of heme binding site of all purified mutants were quite similar to that of the wild-type enzyme, although the fraction of the inactivated form, called "P420", was increased. In the reaction with H₂O₂, only trace amounts of the naphthalene hydroxylation product were detected by gas chromatography. We, therefore, conclude that the three mutants do not exhibit the significant changes in the structural and functional properties from those of wild-type P450cam except for the stability of the axial ligand in the reduced form. The enhanced fluorescence in the whole-cell assay would reflect the enhancement in the oxygenation activity below the detectable limit of the gas chromatography and/or contributions of other reactions catalyzed by the heme iron.

II-E-2 Spectroscopic Characterization of Heme Binding to the Heme Regulatory Motif (HRM) in the Bacterial Iron Response Regulator Protein

ISHIKAWA, Haruto¹; TAKAHASHI, Satoshi¹;
HORI, Hiroshi²; O'BRIAN, Mark R.³;
MORISHIMA, Isao¹; ISHIMORI, Koichiro⁴
(¹Kyoto Univ.; ²Osaka Univ.; ³New York State Univ.;
⁴IMS and Kyoto Univ.)

The heme regulatory motif (HRM) is a common and crucial amino acid sequence for the heme binding in heme-regulated proteins, but the structural characterization of the heme binding to HRM has not yet been extensively accomplished. The bacterial iron response regulator (Irr), controlling the heme biosynthesis by degrading itself in the presence of iron, has one HRM in the sequence. Although the absorption spectrum of Irr in the presence of ferric heme was quite unusual in that the Soret peak was broad with highly blue-shifted and suggestive of the dissociation of the axial ligand from protein, the EPR signals ($g = 2.52, 2.29, 1.90, g = 4$ to 8) and the ν_3 line at 1491 cm^{-1} in the resonance Raman spectrum were characteristic of Cys-ligated hemes. By the mutation of ²⁹Cys to Ala, the EPR signals and the ν_3 line from the Cys-ligated heme diminished, confirming that ²⁹Cys is the axial ligand for ferric heme bound Irr. In sharp contrast to the ferric heme bound Irr, the spectroscopic features of the ferrous heme bound ²⁹Cys → Ala mutant are quite similar to those of wild-type Irr. In addition, the correlation of the stretching modes of $\nu(\text{Fe}-\text{CO})$ and $\nu(\text{FeC}-\text{O})$ for ferrous CO heme bound Irr indicates that the axial ligand trans to CO is histidine. The reduction of the heme iron, therefore, replaces axial ²⁹Cys with histidine. These results provide the first detailed spectroscopic characterization for the heme binding to HRM and provide evidence for redox-dependent axial ligand exchange in Irr.

[*J. Biol. Chem.* Submitted]

II-F Controllable Magnetic Anisotropy of Ultrathin Magnetic Films and Nanowires Using Surface Chemical Techniques

In recent years noble properties of magnetic thin films have extremely attracted scientific and technological interests. Magnetic anisotropy is one of the most important subjects in this field since the origin of perpendicular magnetization is not well understood but is useful for high-density recording media. We are investigating the microscopic mechanism of perpendicular magnetic anisotropy that is stabilized by gaseous adsorption on magnetic film surfaces by means of the synchrotron radiation x-ray magnetic circular dichroism (XMCD) and the visible-light magneto-optical Kerr effect (MOKE) techniques. A goal of these works is spin engineering by which the magnetization of ultrathin metal films and nanowires can be controlled artificially.

II-F-1 X-Ray Magnetic Circular Dichroism Study on NO Adsorbed Co and Ni Ultrathin Films on Cu(001)

NAKAGAWA, Takeshi; WATANABE, Hirokazu; YOKOYAMA, Toshihiko

NO is well known as an effective magnetic killer since NO interacts with magnetic metal surfaces very strongly and the unpaired electron couples with the metal spins antiferromagnetically. In this work, we have investigated the effect of NO adsorption on ultrathin Co and Ni/Cu(001) films from the view point of magnetic anisotropy.

Figure 1 depicts the Ni *L*-edge x-ray magnetic circular dichroism (XMCD) of 5.5 and 9 monolayer (ML) Ni on Cu(001), taken at Beamline 4B in UVSOR. In the case of in-plane magnetized 5.5 ML Ni/Cu(001), both $\theta = 30^\circ$ (close to the in-plane easy axis) and $\theta = 90^\circ$ (along surface normal, hard axis) spectra were taken at a magnetic field of 1000 G and at a temperature of ~ 100 K. The $\theta = 30^\circ$ spectra show noticeable reduction of the magnetization on NO adsorption, while less prominent suppression is found in the $\theta = 90^\circ$ spectra. This finding is similar to the NO/Co/Cu(001) case (not shown). The 9 ML spectra (perpendicular magnetization both before and after NO adsorption) show much less change between clean and NO-adsorbed Ni along the easy axis, being different from the 5.5 ML case.

From the quantitative analysis, it is found that in the in-plane magnetized films of 5.5 ML Ni and 3 ML Co (not shown), the in-plane orbital moments are significantly suppressed on NO adsorption, while perpendicular orbital moments show much less change. The Ni 9 ML films give again almost no change in perpendicular orbital moments. These results imply that NO suppresses the in-plane orbital moment drastically, while the perpendicular orbital moment is much less influenced. Consequently, NO relatively stabilizes perpendicular magnetization effectively.

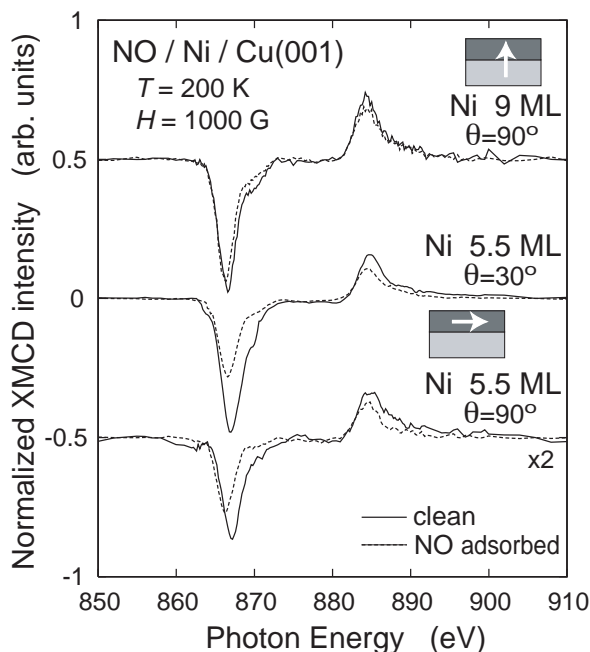


Figure 1. Ni *L*-edge XMCD of 5.5 and 9 ML Ni/Cu(001) before and after NO adsorption. The x-ray incidence angles were $\theta = 30^\circ$ and 90° for 5.5 ML Ni and $\theta = 90^\circ$ for 9 ML Ni.

II-F-2 Is the Perpendicular Magnetic Anisotropy in Ni/Cu(001) Stabilized by the Cu Capping ?

NAKAGAWA, Takeshi; WATANABE, Hirokazu; YOKOYAMA, Toshihiko

The effect of the Cu capping on Ni/Cu(001) films has been investigated by different research groups, and essentially contradictory results were reported. In this work, we have examined the Ni films grown on clean and preoxidized Cu(001) surfaces by means of the MOKE and XMCD. These films consequently show completely different properties concerning the spin reorientation transition, leading to a consequent definite answer for the previous contradictions.

For the Cu-capped Ni films grown on clean Cu(001), the MOKE measurement shows that the critical thickness for the spin reorientation transition of ~ 9 ML before Cu capping is significantly reduced to ~ 6.5 ML after > 0.4 ML Cu capping. The XMCD results clarify that the in-plane orbital magnetic moment is correspondingly suppressed after Cu deposition, while the perpendicular orbital magnetic moment does not vary

irrespective of the presence or absence of the Cu overlayer. On the contrary, for the Cu-capped Ni films grown on preoxidized Cu(001), the opposite trends were basically concluded. MOKE shows that the critical thickness of ~ 5 ML before Cu capping is significantly enlarged to ~ 6.5 ML after Cu capping. The XMCD results clarify that the in-plane orbital magnetic moment is correspondingly enhanced after Cu deposition. Figure 1 shows the orbital magnetic moments from XMCD and the relative hysteresis loss from MOKE, which are in good accordance with each other.

Such different nature originates from the behavior of adsorbed oxygen. Although Ni was deposited onto oxidized Cu(001) in the latter case, the oxygen atoms act as a surfactant and comes up to the surface of the Ni films. Adsorption of oxygen suppresses surface magnetic anisotropy that favors in-plane magnetization much more effectively than clean Ni and even than the Cu/Ni interface. Furthermore, when depositing Cu, oxygen again comes up to the Cu overlayer and locates at the surface, in spite that the O–Ni bond is much stronger than the O–Cu bond. Since no O–Ni interaction remains any more, the Cu-capped Ni films shows similar magnetic properties. The present finding clearly concludes that the modification of the in-plane orbital moment drives the spin reorientation transition.

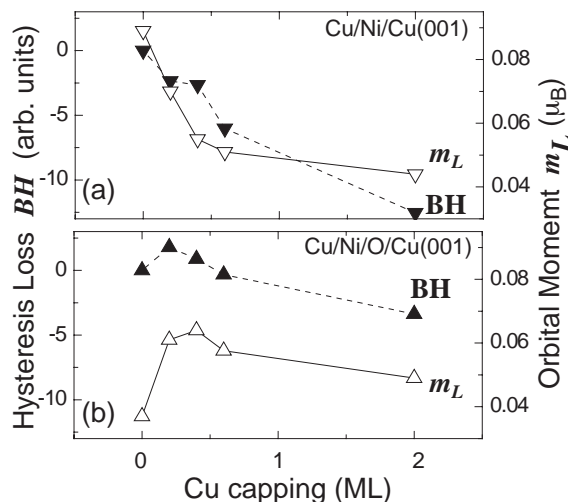


Figure 1. Comparison between the hysteresis losses (open symbols) from MOKE and the orbital magnetic moment (filled symbols) from XMCD for (a) Cu/Ni(5.5 ML)/Cu(001) and (b) Cu/Ni(4.8 ML)/O/Cu(001). The plots demonstrate a one-to-one correspondence between the hysteresis loss and orbital magnetic moment.

II-F-3 Switching of the Magnetic Easy Axis in Pseudo-Nanowire Co on Vicinal Cu(1 1 41) Surface *via* Ag and NO Adsorption

NAKAGAWA, Takeshi; WATANABE, Hirokazu; YOKOYAMA, Toshihiko

It is well known that rod magnets are likely to be magnetized along its axis due to shape anisotropy. Metal thin films grown on stepped surfaces can be regarded as pseudo-nanowires, which are connected at the step edges with each other. These films are found to

exhibit strong uniaxial magnetic anisotropy along the step direction. Weber *et al.* [*Phys. Rev. B* **52**, R14400 (1995)] reported surprising results whereby Ag capping induces the switching of the easy axis of Co on a vicinal Cu surface. In this work, we have tried to confirm the findings on 10 ML Co on Cu(1 1 41) and moreover have investigated the effect of NO adsorption on 7 ML Co on the same substrate by means of the MOKE experiments.

Figure 1 depicts the hysteresis loops recorded by the longitudinal MOKE measurements of 10 ML Co on Cu(1 1 41) (a) before and (b) after 0.2 ML Ag deposition. On clean Co, a normal hysteresis loop was observed along the step, while a double hysteresis with a shift filed can be found in the direction perpendicular to the step. This implies that the magnetic easy axis, which was along the step as in the usual case, rotates by 90° and is perpendicular to the step direction within the surface plane. The previous experiments were confirmed and more detailed information was derived.

Figure 1(c) shows the hysteresis loops of 7 ML Co before and after NO adsorption. Before NO adsorption, clear uniaxial anisotropy is again seen, implying that the easy axis is along the step. After NO adsorption, the hysteresis loop is dramatically changed. There can be found no angular dependence and both the loops taken parallel and perpendicular to the step are identical. Correspondingly, the coercive field is drastically reduced. This implies that the easy axis disappears and the pseudo-nanowire behaves as if it had a fourfold symmetry. The XMCD measurements are in progress.

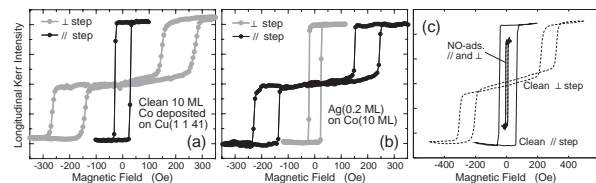


Figure 1. (a,b) Hysteresis loops of 10 ML pseudo-nanowire Co on Cu(11 41) (a) before and (b) after Ag deposition with the magnetic field parallel (black) and perpendicular (gray) to the step; (c) Hysteresis loops of 7 ML pseudo-nanowire Co on Cu(11 41) before and after NO adsorption with the magnetic field parallel (solid) and perpendicular (dashed) to the step.

II-G Molecular and Electronic Structures of Metallofullerenes

The continued interest in radical ions of fullerenes and metallofullerenes has resulted from the discovery of superconductivity in the CT complexes of alkali metals with fullerenes. Spectroscopic information concerning the electronic and spin states of the metallofullerene has been of great interest and obtained by ESR measurements.

II-G-1 Characterization of Ce@C₈₂ and Its Anion

WAKAHARA, Takatsugu¹; KOBAYASHI, Jun-ichi²; YAMADA, Michio¹; MAEDA, Yutaka¹; TSUCHIYA, Takahiro¹; OKAMURA, Mutsuo²; AKASAKA, Takeshi¹; WAECHLICH, Markus³; KOBAYASHI, Kaoru; NAGASE, Shigeru; KATO, Tatsuhisa; KAKO, Masahiro⁴; YAMAMOTO, Kazunori⁵; KADISH, Karl M.⁶
(¹Univ. Tsukuba; ²Niigata Univ.; ³Bryker Japan; ⁴Univ. Electro-Communication; ⁵Japan Nuclear Fuel Cycle Development Inst.; ⁶Univ. Huston)

[*J. Am. Chem. Soc.* **126**, 4883–4887 (2004)]

Ce@C₈₂ is isolated by HPLC and the cage symmetry is determined as C_{2v} by measuring the ¹³C NMR spectra of its anion. The ¹³C NMR peaks of [Ce@C₈₂]⁻ show temperature-dependent shifts ascribed to the *f* electron remaining on the Ce atom. Both Ce@C₈₂ and [Ce@C₈₂]⁻ are ESR silent because of the highly anisotropic *g* matrix as well as of the fast relaxation process originating from the orbital angular momentum of the *f* electron. This is the complementary relationship to the observation of the paramagnetic shift in ¹³C NMR. [Ce@C₈₂]⁻ has a lower stability in air than [La@C₈₂]⁻.

II-G-2 Isolation and Crystallographic Characterization of the La@C₈₂ Derivative

MAEDA, Yutaka¹; MATSUNAGA, Yoichiro²;

WAKAHARA, Takatsugu²; TAKAHASHI, Satomi³; TSUCHIYA, Takahiro²; ISHITSUKA, Midori O.²; HASEGAWA, Tadashi¹; AKASAKA, Takeshi²; LIU, Michael T. H.⁴; KOKURA, Kisato⁵; HORN, Ernst⁵; YOZA, Kenji⁶; KATO, Tatsuhisa; OKUBO, Shingo; KOBAYASHI, Kaoru; NAGASE, Shigeru; YAMAMOTO, Kazunori⁷
(¹Tokyo Gakugei Univ.; ²Univ. Tsukuba; ³Niigata Univ.; ⁴Univ. Prince Edward Island; ⁵Rikkyo Univ.; ⁶Bruker AXS K. K.; ⁷Japan Nuclear Cycle Development Inst.)

[*J. Am. Chem. Soc.* **126**, 6858–6859 (2004)]

The photochemical reaction of La@C₈₂ with 2-adamantane-2,3-[3H]-diazirine affords adduct **2**, La@C₈₂(Ad), in a quantitative and highly selective manner. The structure of compound **2** is confirmed by ESR, MS, and UV-Vis-NIR spectroscopies, and the first X-ray crystallographic characterization of an endohedral monometallofullerene derivative is reported. We have reported that the relatively higher reactivity of endohedral metallofullerenes is due to their electronic properties. The reaction EPR spectra reveal the formation of several regioisomers with different La isotopic splittings. In contrast, the regiospecific addition reaction of La@C₈₂ with 2-adamantane-2,3-[3H]-diazirine (**1**) affords the first single isomer which has been successfully isolated. Reported here is the first isolation and crystallographic characterization of a paramagnetic endohedral monometallofullerene derivative of the selective La@C₈₂ reaction.

II-H High Field and Pulsed Electron Spin Resonance Spectroscopy

Electron paramagnetic resonance (EPR) spectroscopy has been a powerful technique for the characterization of radical species. The modern development of EPR spectroscopy enables us to investigate the heterogeneous and disordered system in detail. Especially the high frequency and pulsed EPR methods achieve the substantial resolution enhancement of spectrum. The advanced EPR spectroscopy is applied to study on the spin state in the heterogeneous system.

II-H-1 W-Band EPR Detection of the Manganese Multiline in the S₂ State of Cyanobacterial Photosystem II Single Crystal

KAWAMORI, Asako¹; SHEN, Jian-Ren²; MINO, Hiroyuki³; FURUKAWA, Ko; MATSUOKA, Hideto; KATO, Tatsuhisa

(¹Kwansei Gakuin Univ.; ²Okayama Univ.; ³Nagoya Univ.)

The multiline signal of the manganese cluster in oxygen evolving complex of photosystem II in the S₂-state was detected in the single crystal form of *thermosynechococcus vulcanus* by W-band EPR measurement.

The distinct 21 lines with irregular spacing were identified, which is due to the hyper fine coupling (hfc) with manganese ($I = 5/2$) nuclear spins. The combination of the orientation of hfc- and g -tensors among the multi-sites of manganese cluster strongly affected the appearance of spectrum, and the overlapped hfc structure was smeared out in some orientation of the single crystal. The peculiar spectral patterns in various orientations of the single crystal were well simulated under the assumption of the trimer-monomer structure for the manganese cluster, and the principal values and the direction of the principal axis of an effective g -tensor were determined. The g_z component of the g -tensor was deduced as to be perpendicular to the two-fold axis relating the dimer structure in one subunit of the protein crystal.